**Review**

# PHOTONICS Research

# Ultrafast fiber lasers mode-locked by two-dimensional materials: review and prospect

Tian Jiang,[1,*,†] (iD) Ke Yin,[2,†] Cong Wang,[3,†] Jie You,[2] Hao Ouyang,[1] Runlin Miao,[1] Chenxi Zhang,[1] Ke Wei,[1] Han Li,[1] Haitao Chen,[1] Renyan Zhang,[1] (iD) Xin Zheng,[2] Zhongjie Xu,[1] Xiangai Cheng,[1] and Han Zhang[3,4] (iD)

[1]College of Advanced Interdisciplinary Studies, National University of Defense Technology, Changsha 410073, China
[2]National Innovation Institute of Defense Technology, Academy of Military Sciences China, Beijing 100071, China
[3]Shenzhen Engineering Laboratory of Phosphorene and Optoelectronics and Key Laboratory of Optoelectronic Devices and Systems of Ministry of Education and Guangdong Province, Shenzhen University, Shenzhen 518060, China
[4]e-mail: hzhang@szu.edu.cn
*Corresponding author: tjiang@nudt.edu.cn

The year 2019 marks the 10th anniversary of the first report of ultrafast fiber laser mode-locked by graphene. This result has had an important impact on ultrafast laser optics and continues to offer new horizons. Herein, we mainly review the linear and nonlinear photonic properties of two-dimensional (2D) materials, as well as their nonlinear applications in efficient passive mode-locking devices and ultrafast fiber lasers. Initial works and significant progress in this field, as well as new insights and challenges of 2D materials for ultrafast fiber lasers, are reviewed and analyzed.    © 2019 Chinese Laser Press

https://doi.org/10.1364/PRJ.8.000078

## 1. INTRODUCTION

Ultrafast fiber lasers (UFLs), which deliver pulses with extremely short durations (e.g., on the order of femtoseconds or picoseconds), have been proved as the most powerful tool for various and crucial applications such as strong-field physics, nonlinear optics, precision metrology, and ultrafine material processing. One distinguishing property of rare-earth-doped fibers is the large gain bandwidth (i.e., tens of nanometers), making possible the generation of ultrafast mode-locked laser pulses (∼100 fs). In order to achieve the mode-locking response, cavity longitudinal modes must be forced to lock together by either active electro-optic modulators or passive saturable absorbers (SAs). Comparatively, a passively mode-locked fiber laser using a real SA has the significant advantages of self-starting operation, low cost, high stability, and being maintenance-free.

Currently, the most prevalent absorber technology is the molecular beam epitaxy (MBE)-grown semiconductor SA mirror (SESAM) [1], which is widely applied in semiconductor lasers, UFLs, and solid-state lasers. However, SESAM has its own limitations, including long recovery time (∼picosecond level), narrowband operation (<100 nm), sophisticated fabrication, and a low damage threshold. Therefore, the pursuit of an ideal SA, the key module of a passively mode-locked fiber laser, has long been the goal of scientific researchers.

Two-dimensional (2D) materials, also denoted as atomic layered materials, define a new material morphology where single or few layers of atoms gather together in one direction, while in two other directions, they keep uniform and crystal-like expansions. With the reduction in physical dimension, 2D materials bring totally different energy band structures when compared to their bulk states, and possess unique optical and electronic characteristics [2–5] that have been employed in applications of microelectronics devices [6], biomedicine [7], energy [8], and chemistry [9]. As summarized in this review, one of the most exciting things is that they could be used as passive SAs, the mode-lockers for UFLs. The origin of saturable absorption in 2D materials is similar to SESAM, in that the absorption of injected light can be saturated under strong excitation due to the depletion of final states (i.e., Pauli blocking).

Ignited by Bao et al. [10] and Sun et al. [11,12], who reported the initial UFLs mode-locked by graphene in 2009, a rapid exploration of the 2D material family as efficient fiber SAs has occurred. The most widely investigated 2D materials in this field are graphene [13,14], topological insulators (TIs) [15,16], transition metal dichalcogenides (TMDs) [17,18], and black phosphorus (BP) [19,20]. In addition, some newly emerging 2D materials continue to join the 2D family, like MXenes [21,22], bismuthene [23], and antimonene [24], all reported recently. The profusion of 2D materials together with diverse fiber integration methods brings quite a great flexibility in fabricating fiber SAs with unique and controllable parameters, allowing for broad bandwidth, ultrafast recovery, high damage

threshold, low saturable influence, etc. In combination with rich rare-earth-doped fiber lasers in different wavelength regions, the development of UFLs mode-locked by 2D nanomaterials has been greatly facilitated over the last decade [25–29].

In this paper, we cover the state of art of UFLs mode-locked by 2D materials. In Section 2, a brief introduction to dominant 2D materials is made, including their atomic structures, energy band structures, linear and nonlinear absorptions, carrier lifetimes, etc. Related experimental approaches for fabricating these 2D materials and fiber SAs are also mentioned. In Section 3, the historical first demonstrations of UFLs mode-locked by 2D materials are presented. In Section 4, some important and interesting progress in recent years is summarized, mainly focusing on pulse width, repetition rate, and stability characteristics. In Section 5, new insights and current challenges regarding 2D materials are discussed.

## 2. 2D MATERIAL FAMILY FOR UFLS

In the fields of ultrafast photonics, 2D materials are characterized by their broadband saturable absorptions [30–32], ultrafast recovery [33–35], large nonlinear refractive indices [36,37], and potential as outstanding mode-lockers for UFLs. What follows is a brief overview of 2D materials' atomic structures, bandgap structures, and recovery times. Table 1 shows a brief comparison of the 2D material family. Later in this section, corresponding material preparation and fiber integration techniques are also introduced.

### A. 2D Materials
#### 1. Graphene
Graphene, viewed as the pioneer of 2D materials, is a single layer of carbon atoms arranged in a 2D honeycomb lattice [14], facilitating great potential in the application of UFLs. Benefiting from its gapless Dirac cone [13], monolayer graphene is calculated to possess about 2.3% absorption of incident visible to infrared (IR) light. Graphene is special in that it enjoys ultrashort recovery time (<200 fs), low saturable

absorption (~10 MW/cm$^2$ [38]), great relative modulation depth (>60% per layer [10]), and wavelength-independent operation (ranging from the visible to the terahertz), allowing it to operate efficiently for the generation of broadband ultrafast laser pulses.

#### 2. TIs
TIs define a new kind of material with nontrivial symmetry-protected topological order that behaves as insulators in their interior but whose surfaces contain gapless conducting states [15,16,50]. A small indirect bulk bandgap of 0.2–0.3 eV gives TIs a strong graphene-like broadband nonlinear response from the visible to the mid-IR. The lifetime of their phonon-induced carriers is short of several picoseconds, also making them useful for ultrafast light modulators. Three kinds of TIs, namely, $Sb_2Te_3$, $Bi_2Se_3$, and $Bi_2Te_3$, are the most widely used TI SAs.
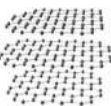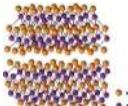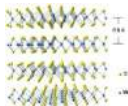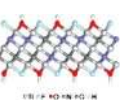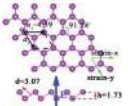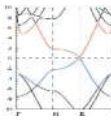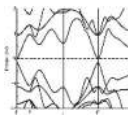
#### 3. TMDs
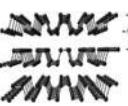TMDs are a class of more than 40 different semiconductors that share a formula of $MX_2$, where $M$ stands for a transition metal (e.g., Mo, W, Ti, Nb) and $X$ stands for a chalcogen (e.g., S, Se, or Te) [51,52]. In a TMD monolayer, the single transition metal layer is sandwiched between the two chalcogen layers, showing graphene-like layered structure. As for different monolayer TMDs, they have energy bandgaps varying from 1 to 2.5 eV. Surprisingly, the subbandgaps created by the edge states of TMDs allow efficient absorptions of light with photon energy much lower than their normal bandgaps [53,54]. Meanwhile, the short recovery times of TMDs are several picoseconds, which are also fast enough for ultrafast light modulation. For example, $MoS_2$, $MoTe_2$, $WSe_2$, and $WS_2$ have been widely used for UFLs in 1.5 and 2 μm wavelength regions.

#### 4. BP
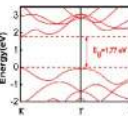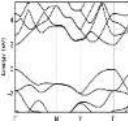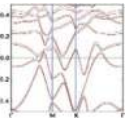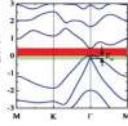BP is a thermodynamically stable allotrope of phosphorus at room temperature [19,55]. Like graphene, each phosphorus atom in BP is connected to three adjacent phosphorus atoms, forming a stable six-atom linked ring structure. The difference is that the BP structure is puckered, which reduces its

## Table 1. 2D Material Family for UFLs[a,b]

| Type | Graphene [38,39] | TIs [16,40,41] | TMDs [42–44] | BP [45,46] | MXenes [47] | Bismuthene [24,48,49] |
|---|---|---|---|---|---|---|
| Atomic structure |  |  |  |  |  |  |
| Band structure (monolayer) |  |  |  |  |  |  |
| Bandgap | 0 eV (monolayer) 0.25 eV (bilayer) | 0–0.7 eV | 1–2.5 eV | 0.35–2 eV | <0.2 eV | ~0.5 eV (monolayer) |
| Carrier lifetime | Fast: <200 fs Slow: ~1 ps | Fast: 0.3–2 ps Slow: 3–23 ps | Fast: ~1–3 ps Slow: 70–400 ps | Fast: 360 fs Slow: 1.36 ps | – | Fast: 3 ps Slow: 420 ps |

[a]Atomic and electronic band structures of $Bi_2Se_3$, $MoS_2$, and $Ti_3CNT_x$ ($T$ = F, OH) are selected to represent TIs, TMDs, and MXenes, respectively.
[b]Bandgaps and carrier lifetimes of TIs and TMDs are value ranges from a variety of materials.

symmetry and brings an angle-dependent nonlinearity [56]. It has tunable direct bandgaps varying from 0.35 eV (bulk) to 2 eV (monolayer), indicating its broadband nonlinear response deep into the mid-IR [57,45], which has been widely used for UFLs as well [58,59]. Research shows that nanosheet BP has a wavelength-dependent recovery time of 0.36 to 1.36 ps excited with photon energies from 1.55 to 0.61 eV [60]. It should be noted that BP would be oxidized when exposed in ambient conditions and needs encapsulation for scaling its long-term stability [61].

### 5. MXenes

MXenes represent a new class of 2D transition metal carbides, carbonitrides, or nitrides whose chemical formula is $M_{n+1}X_nT_x(n = 1-3)$. Here, $M$ stands for transition metals (Sc, Ti, Zr, Hf, V, Nb, Ta, Cr, Mo, etc.), $X$ is carbide and/or nitride, and $T_x$ represents surface terminations (F, O, OH, etc.) [22,62]. Few-layer $Ti_3C_2T_x$ has an indirect energy bandgap of <0.2 eV and a low absorption of ~1%/nm. Stacking of 2D MXene materials generally occurs through van der Waals interaction without internal surface termination, as in the cases of graphene, phosphorene, and TMDs. A recent study showed that the main features observed in MXene monolayers were well conserved in stacked ones [47], indicating that well-functioning fiber SAs could be made using MXenes, thus avoiding the troublesome processes of monolayer dispersion.

### 6. Bismuthene

Due to its distinct electronic and mechanical properties, as well as its strong stability, bismuthene has attracted tremendous research interest [23,48]. Recent research shows that the layer-dependent optical bandgap of beta-bismuthene ranges from almost 0 to 0.55 eV, suggesting that it is a promising broadband optical material from the near-IR to the terahertz regions [24]. The short recovery time of bismuthene is 2.8 ps, which also indicates it is a potential ultrafast SA.

### 7. Other Materials

The aforementioned 2D materials offer distinct, yet complementary properties and hence, new opportunities for optical applications in UFLs [63–65]. But these are not enough, since better SAs with enhanced optical properties, such as much shorter carrier lifetimes, higher damage thresholds, and larger modulation depths are always desired. On the one hand, explorations for new 2D materials will never stop. On the other hand, modification of existing materials also provides an opportunity. The possibility of combining different 2D materials to form van der Waals heterostructures offers an exciting prospect for a wide range of new engineerable photonic devices [66,67]. This overcomes the intrinsic drawbacks of single materials, while enhancing performance greatly [68,69]. Recently, several UFLs mode-locked by heterostructure SAs have been reported [70,71].

## B. Preparation and Characterization of 2D Materials

To summarize, there are many physical or chemical techniques used to obtain 2D materials, which can be classified into two categories, namely, top-down exfoliation and bottom-up growth [72]. Typical approaches regarding exfoliation are mechanical exfoliation (ME) [73], liquid-phase exfoliation

(LPE) [74], and ion-intercalation exfoliation [75]. Meanwhile, chemical vapor deposition (CVD) [76], pulsed laser deposition (PLD) [77], pulsed magnetron sputtering (PMS) [78], and MBE [28] are representative growth techniques.

At the same time, plenty of measurement techniques have been introduced to characterize 2D materials. To analyze the atomic composition and structural characteristics, the X-ray diffractometer, Raman scattering spectroscopy, and photoluminescence measurements are often used. Scanning electron microscopy (SEM), atomic force microscopy (AFM), and atomic resolution scanning transmission electron microscopy (STEM) are used to characterize the morphology. With Z-scan or P-scan measurements, it is possible to measure the third-order nonlinear coefficients and saturable absorptions directly. Pump–probe spectroscopy is used to analyze the carrier lifetime. Recently, both Z-scan [36] and pump–probe spectroscopy [79] have been shifted to mid-IR regions. Micro pump–probe spectroscopy has also been promoted as an efficient tool to investigate 2D materials' carrier transportation on the scale of micrometers [80,81].

## C. Fiber Integration with 2D Materials

To fabricate SAs for all-fiber mode-locked UFLs, 2D materials must be transferred [82] or deposited [83] onto optical fibers, achieving sufficient interaction with intracavity laser light. Meanwhile, 2D materials could be mounted onto a transparent plate or a high-reflectivity mirror. In these cases, UFLs with non-all-fiber formats could also be established with free-space couplings. Both polarization-maintaining (PM) and non-PM fibers could be used for building these UFLs with 2D materials. Figure 1 shows some popular fiber coupling schemes. Briefly, these couplings could be summarized into two kinds of schemes: transmission coupling [Figs. 1(a)–1(c)] and evanescent-wave coupling [Figs. 1(d)–1(g)].

### 1. Transmission Coupling

As shown in Fig. 1(a), the most common transmission coupling sandwiches SA materials between two fiber ends directly. Large area uniform 2D materials like ME-prepared graphene, CVD-grown graphene or TMDs, and MBE-grown TIs could be easily integrated with transferring methods [82]. Monolayer or few-layer nanosheet materials embedded in thin organic polyvinyl alcohol (PVA)/polymethyl methacrylate (PMMA)/polydimethylsiloxane (PDMS) films could be sandwiched too. For nanosheets in solutions, direct optical heat deposition to a fiber end is
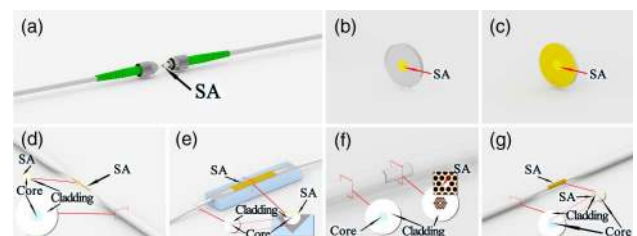


**Fig. 1.** Fiber integration with 2D materials. (a)–(c) Transmission coupling; (d)–(g) evanescent-wave coupling; 2D materials are deposited or transferred on (a) fiber ends, (b) transparent plate, (c) reflection mirror, (d) tapered fiber, (e) side-polished fiber, (f) photonic crystal fiber, and (g) cladding-etched fiber.

often used. In general, these methods are simple, and commercial fiber connector/physical contact (FC/PC) or fiber connector/angled physical contact (FC/APC) could be used directly. Figures 1(b) and 1(c) depict the cases when 2D materials are transferred or deposited onto a transparent plate or a high-reflectivity mirror, respectively. Besides, discrete optical components such as lenses must be adopted, resulting in free-space coupling with fibers. It should be noted that transmission coupling does have its disadvantages, such as a low damage threshold.

### 2. Evanescent-Wave Coupling

To scale the damage threshold of fiber SAs, evanescent-wave coupling usually provides a better choice. In this condition, the fiber-guided laser light in the core originally would leak out and interact with 2D materials on the side. The main four evanescent-wave couplings are sketched in Fig. 1, including tapered fiber [84], side-polished fiber [85], photonic crystal fiber [86], and cladding-etched fiber [87]. Both side-polished fiber [88] and photonic crystal fiber [89] have already been demonstrated to support high-power mode-locking operations.

After integration, a fiber SA component should be characterized further with methods including linear transmission spectroscopy and fiber-balanced twin-detector measurement [90], reflecting the fiber SAs' modulation depths and nonsaturable loss. These tests are always important and indispensable because they reflect whether the integration process has been successful or not.

## 3. FIRST DEMONSTRATIONS OF UFLS MODE-LOCKED BY 2D MATERIALS

As discussed in Section 2, 2D materials are innate broadband SAs, enabling the realization of mode-locked UFLs at luxuriant wavelengths. The numerous laser transitions available from trivalent rare-earth ions like $Yb^{3+}$, $Er^{3+}$, $Tm^{3+}$, and $Ho^{3+}$ lend them the ability to generate light over a wide selection of wavelengths [91–94]. Despite different kinds of fibers, fibers made of silica and fluoride ($ZrF_4 – BaF_2 – LaF_3 – AlF_3 – NaF$, ZBLAN) glasses are the most widely used. Figure 2 sketches the very initial demonstrations of 2D materials-based UFLs at 1.0, 1.5, and 2.0 μm (silica), and 3.0 μm (ZBLAN) over the last decade.

Bao et al. reported the first graphene $Er^{3+}$-doped fiber laser (EDFL) at 1550 nm [10] in 2009. From Fig. 3(a), one can see

**Fig. 2.** First demonstrations of UFLs mode-locked by 2D materials at different wavelengths.
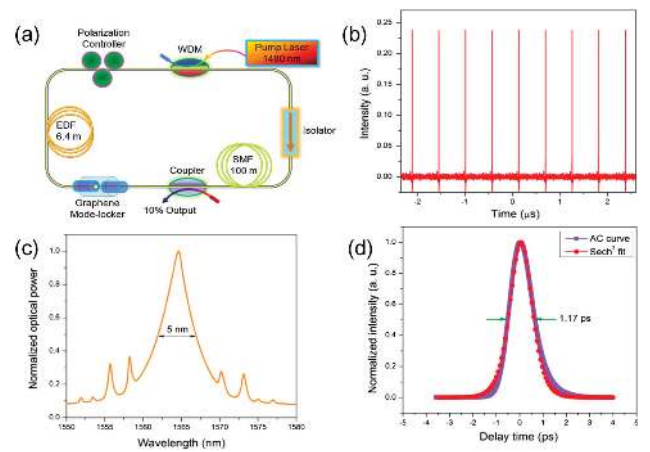
**Fig. 3.** CVD-grown graphene mode-locked EDFL [10]. (a) Laser configuration; (b) output pulse train; (c) output laser spectrum; (d) autocorrelation trace. Reproduced with permission, Copyright 2009, Wiley-VCH.

that a ring-cavity EDFL was mode-locked by a CVD-grown graphene film sandwiched between two fiber ends. In this case, a stable and regular soliton pulse train was generated, along with a repetition rate of 1.79 MHz and output power of 2 mW. The output pulses had a temporal width of 756 fs and a spectral bandwidth of 5 nm, indicating the ultrafast characteristics. Soon after that, mode-locked pulses at 1576.3 nm with a pulse width of 415 fs and a repetition rate of 6.84 MHz were obtained by Zhang et al. from a dispersion-managed cavity fiber laser [95]. At the end of 2009, Sun et al. also demonstrated their first work on an ultrafast EDFL mode-locked by monolayer and few-layer graphene flakes [12]. They proposed that high-performance ultrafast pulses could also be obtained with a graphene–PVA composite fabricated by using wet-chemistry techniques. These works in 2009 were pioneering, opening the door for UFLs mode-locked by 2D materials.

As aforementioned, it is feasible to transplant mode-locking operation to other wavelengths, since gapless graphene makes it a natural broadband SA. Just one year later, Zhao et al. reported an ultrafast $Yb^{3+}$-doped fiber laser (YDFL) mode-locked by a few-layer CVD-grown graphene film. They obtained dissipative soliton pulses at 1069.8 nm with a spectral bandwidth of 1.29 nm and a pulse width of 580 ps [96]. In 2012, Zhang et al. reported the first graphene–PVA composite mode-locked $Tm^{3+}$-doped fiber laser (TDFL) at 1940 nm [97]. The laser output pulses had temporal widths of 3.6 ps and a pulse energy of ~0.4 nJ at a repetition rate of 6.46 MHz. UFLs in this wavelength region are important because of eye-safe operation and their potential as laser scalpels. In 2015, a graphene mode-locked $Ho^{3+}$-doped fiber laser (HDFL) at 2107 nm with a pulse width of 1.8 ps was further demonstrated [98].

In the meantime, researchers also paid much attention to other kinds of 2D materials [3,72]. TIs, TMDs, BP, MXenes, and bismuthene were successively fabricated as fiber SAs and applied into mode-locked UFLs. To the best of our knowledge, the first demonstration of UFLs mode-locked by TI – $Bi_2Te_3$ was in 2012 [99], TMD – $MoS_2$ in 2014 [100], BP in 2015 [101], MXene [47] and bismuthene [102] in 2017.
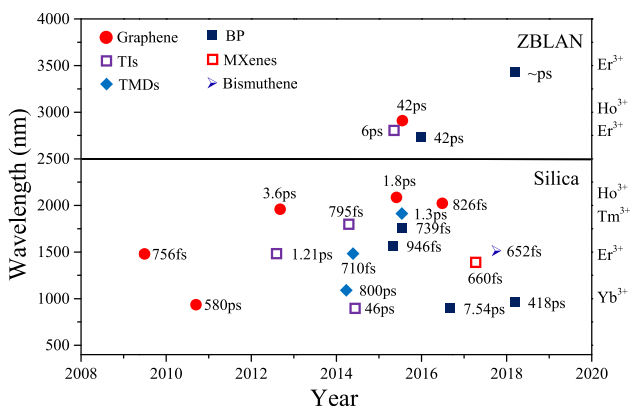
Interestingly, almost all these initial demonstrations were at 1.5 μm except TMD – $MoS_2$ at 1 μm [100], which might benefit from the telecommunications boom. Meanwhile, these 2D materials were also investigated to explore the broadband lasing wavelengths like graphene [103–108]. In summary, not only graphene, but also TIs, TMDs, and BP have been used for the generation of 1, 1.5, and 2.0 μm ultrafast pulses in these corresponding silica fiber lasers. Note that these demonstrations of broadband SA characteristics were indirect because 2D materials were prepared by different groups, even with different methods. In 2014, Fu *et al.* put forward a direct demonstration of graphene's broadband saturable absorption by inserting a single-fiber SA into three codoped fiber lasers: YDFL, EDFL, and $Tm^{3+}$, $Ho^{3+}$ (THDFL), respectively [30]. Thus, mode-locked pulses with center wavelengths of 1035, 1564, and 1908 nm were achieved.

Since graphene, Tis, and BP are gapless or have small energy bandgaps, as introduced in Section 2, they could also be used for mid-IR mode-locking operations. However, silica fiber does not work in the mid-IR due to its huge absorption. The adoption of fluoride ZBLAN fibers for generating ultrafast pulses opens up another playground in the mid-IR for the nonlinear studies of 2D materials. But due to the lack of mid-IR fiber components, current mid-IR UFLs had to adopt non-all-fiber formats limited by a free-space coupling scheme.

In 2015, Yin *et al.* designed the first mid-IR UFL mode-locked by 2D materials [109]. The linear-cavity UFL adopted a piece of $Ho^{3+}$-doped ZBLAN fiber as the gain fiber and a high-reflection gold mirror covered with TI – $Bi_2Se_3$ nanosheets as the SA mirror. The output pulses had a repetition rate of 10.4 MHz, a pulse width of ∼6 ps, and a center wavelength of 2830 nm. Soon after that in 2015, Zhu *et al.* also reported the first mid-IR graphene mode-locked $Er^{3+}$-doped ZBLAN fiber laser at 2.78 μm [110]. A CVD-grown four-to-six layer graphene was transferred onto a gold mirror as the SA. The output had a pulse width of 42 ps and a repetition rate of 25.4 MHz. Few-layer BP SA mirrors have also been built for mid-IR mode-locked UFLs since 2016 [111,112]. In 2016, Qin *et al.* transferred mechanically exfoliated BP flakes onto a gold mirror as a BP SA mirror [111]. The excellent performance of the BP SA mirror in the mid-IR brought stable mode-locked pulses at 2783 nm with a maximum output power of 613 mW, a repetition rate of 24 MHz, and a pulse width of 42 ps. A recent work showed that BP could even be used to modulate lasing at 3489 nm in an $Er^{3+}$-doped ZBLAN fiber laser [112], resulting in a stable mode-locked pulse train with a repetition rate of 28.91 MHz.

## 4. SIGNIFICANT PROGRESS OF UFLS MODE-LOCKED BY 2D MATERIALS

Most of these aforementioned initial UFLs mode-locked by 2D materials are proof-of-concept demonstrations. In fact, their lasing performances are hard to satisfy diverse applications. Therefore, more crucial parameters like SA modifications, cavity dispersion and nonlinearity management, coupling ratio, and gain adjustments are often adopted to improve laser performance. In the following, representative high-performance UFLs mode-locked by 2D materials are reviewed from three

aspects: toward shorter pulse widths, higher repetition rates, and better stabilities. Due to the immature ZBLAN fiber components [113], high-performance mode-locked mid-IR fiber lasers are rare. Therefore, we focus on silica fiber-based UFLs in this section.

### A. Short Pulse Width
The output pulse width of a mode-locked fiber laser depends mainly on its spectral bandwidth and chirp [114]. In fact, the broadband saturable absorption feature of 2D materials could modulate all longitude modes within the whole gain bandwidth of rare-earth ions, leading to desirable ultrafast pulses. When the laser cavity operates in the anomalous dispersion regime, mode-locked pulses can easily evolve into femtosecond solitons, considering the dispersion is comparable to nonlinearity [115].

Based on numerical simulations, Jeon *et al.* found that in a mode-locked UFL, the adoption of SAs with larger modulation depth could induce the temporal shortening of output pulses [116]. Considering that monolayer 2D materials' absorption is low, the problem is how to improve the modulation depth of a 2D material SA. In 2015, Sobon *et al.* put forward a stacking method for monolayer graphene to achieve the desired number of layers [117]. They demonstrated that by increasing the layer numbers, the graphene SA's modulation depth increased, and the output pulse width decreased. This idea of engineering modulation depth by modifying layer numbers was soon adopted in other kinds of 2D materials like TI – $Bi_2Se_3$ [118] and TMD – $MoS_2$ [119].

In order to shorten the mode-locking pulse width, dispersion management is also indispensable. By adopting gain and passive fibers with opposite dispersions [120] or inserting a dispersion compensation grating [121], the net cavity dispersion could be minimized. Indubitably, external pulse compression is a promising alternative. A fiber chirp pulse amplification (CPA) chain can not only scale up pulse energy, but also induce broadening of the amplified spectrum, leading to a much shorter pulse width after compression. Representative results of UFLs mode-locked by 2D materials at short pulse widths are presented in Table 2.

The shortest pulse width (88 fs) output directly from a graphene mode-locked EDFL was reported by Sotor *et al.* in 2015 [122]. A 60-layer CVD-grown graphene/PMMA composite was sandwiched between two fiber ends as an SA. With dispersion compensation, the ring-cavity EDFL had a net dispersion of $-0.0015 ps^2$, resulting in a stretched mode-locking operation at 1545 nm with a spectral bandwidth of 48 nm. Also utilized with CVD-grown graphene films, shortest pulse widths of 603 fs at 1940 nm [123] and 190 fs at 2059 nm [124] were reported. However, due to the lack of dispersion engineering, the graphene mode-locked ZBLAN fiber laser at 2784.5 nm had a long pulse width of 42 ps [110].

With all-fiber CPA systems, ultrafast pulses shorter than 24 and 260 fs at 1560 and 1968 nm were obtained [125,126], respectively. Figure 4 shows the corresponding result when the shortest pulse width of 24 fs was realized [125]. As presented in Fig. 4(a), the laser system consisted of only two types of PM fibers, ensuring simplicity and stability. A 30-layer graphene/polymer composite as described in detail in Ref. [117], was used as the fiber SA in the mode-locked EDFL. The output

**Table 2.  UFLs Mode-Locked by 2D Materials with Short Pulse Widths**

| Laser Configuration | SA | Pulse Width | Wavelength | Spectral Bandwidth | Ref. |
|---|---|---|---|---|---|
| Dispersion compensated ring-cavity EDFL | 60-layer CVD-grown graphene | 88 fs | 1545 nm | 48 nm | [122] |
| Ring-cavity TDFL | 24-layer CVD-grown graphene | 603 fs | 1940 nm | 6.6 nm | [123] |
| Dispersion compensated ring-cavity HDFL | Few-layers graphene | 190 fs | 2059 nm | 53.6 nm | [124] |
| Linear-cavity $Er^{3+}$-doped ZBLAN fiber laser | 4–6 layer CVD-grown graphene | ~42 ps | 2784.5 nm | 0.21 nm | [110] |
| Ring-cavity EDFL + EDFA | 30-layer CVD-grown graphene | 224 fs/24 fs[a] | 1560 nm | 11.5 nm/136 nm[b] | [125] |
| Ring-cavity TDFL + TDFA | 12-layer CVD-grown graphene | 656 fs/260 fs[a] | 1968 nm | 9.4 nm/15 nm[b] | [126] |
| Ring-cavity YDFL | 250 nm PMS-deposited TI – $Bi_2Te_3$ | 5.3 ps | 1036.7 nm | 8.28 nm | [78] |
| Ring-cavity EDFL | PLD-prepared TI – $Sb_2Te_3$ | 70 fs | 1542 nm | 63 nm | [127] |
| Ring-cavity EDFL | Bulk-structured TI – $Bi_2Te_3$ | 795 fs | 1935 nm | 5.64 nm | [104] |
| Linear-cavity $Ho^{3+}$-doped ZBLAN fiber laser | LPE-prepared TI – $Bi_2Te_3$ | 6 ps | 2830 nm | 10 nm | [109] |
| Ring-cavity EDFL | CVD-grown TMD – $WSe_2$ | 163.5 fs | 1557.4 nm | 25.8 nm | [128] |
| Ring-cavity EDFL | PLD-prepared TMD – $WS_2$ | 67 fs | 1540 nm | 114 nm | [129] |
| Ring-cavity EDFL | LPE-prepared BP | 102 fs | 1555 nm | 40 nm | [130] |
| Ring-cavity TDFL | ME-prepared BP | 739 fs | 1910 nm | 5.8 nm | [108] |
| Linear-cavity $Ho^{3+}$-doped ZBLAN fiber laser | LPE-prepared BP | 8.6 ps | 2866.7 nm | 4.35 nm | [131] |
| Ring-cavity EDFL | LPE-prepared bismuthene | 193 fs | 1561 nm | 14.4 nm | [132] |
| Ring-cavity EDFL | MXene-$Ti_3C_2T_x$ | 159 fs | 1555 nm | 22.2 nm | [133] |

[a]Pulse widths of 224 and 656 fs were obtained from oscillators, while 24 and 260 fs were obtained after amplifiers.

[b]Spectral bandwidths of 11.5 and 9.4 nm were obtained from oscillators, while 136 and 15 nm were measured after fiber amplifiers.

pulse from the oscillator had the shortest temporal width of 224 fs, associated with a lasing wavelength of 1560 nm and a spectral bandwidth of 11.5 nm. After amplification with an $Er^{3+}$-doped fiber amplifier (EDFA) and compression in the gain fiber, the fiber laser system delivered few-cycle optical pulses with a pulse width short of 24 fs and a spectral bandwidth of 136 nm.

As illustrated in Table 2, one can acquire the shortest output pulse widths for the UFLs mode-locked by other kinds of 2D materials. These results are generated directly from mode-locked laser oscillators without amplification and compression. In the 1.5 μm wavelength region, the shortest output pulses mode-locked by TIs, TMDs, BP, bismuthene, and MXenes were 70 fs [127], 67 fs [129], 102 fs [130], 193 fs [132], and 159 fs [133], respectively. These works demonstrated that other 2D materials also had the ability to generate ~100 fs

ultrafast laser pulses. Comparatively, the output pulses at other wavelengths like 1 and 2 μm are still much longer than pulses at 1.5 μm, indicating much more work is required to shorten pulses in the future. Meanwhile, robust fiber amplifiers operating in these wavelength ranges are also required to scale up pulse energy and peak power, and further shorten the pulse width.

### B. High Repetition Rate
The pursuit of higher repetition rates is another important aspect. In particular, lasers with repetition rates from several to hundreds of gigahertz are important for high-speed optical communication systems and microwave generation. The short recovery times of 2D materials make them good candidates for gigahertz pulse generation.

Table 3 shows the representative results of high repetition rate UFLs mode-locked by 2D materials. For fundamental mode-locking operation, the repetition rate of the pulse train is the same as the longitudinal mode spacing, whose increment can only be achieved by reducing cavity length. In 2012, Martinez *et al.* reported a graphene mode-locked EDFL with a ~1 cm linear cavity, whose pulse repetition rate was 9.67 GHz [134]. In 2015, Wu *et al.* also demonstrated a $MoS_2$-based short-cavity EDFL at a fundamental repetition rate of 463 MHz [139]. However, due to the fiber gain limitation, short-cavity configuration is difficult to improve the repetition rate further (e.g., >10 GHz).

By inserting a comb filter like Fabry–Perot (FP) filter or microknot filter into a fiber laser cavity to form a composite cavity, it is also possible to increase output repetition rate by filtering out some longitudinal modes [114]. In 2015, Qi *et al.* reported the generation of a 100 GHz pulse train in an EDFL by using a graphene tapered fiber SA and an FP filter [136].
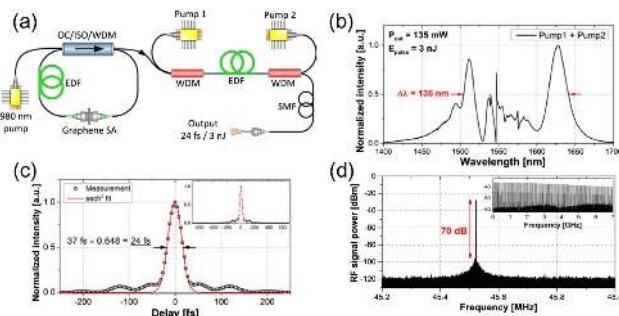


**Fig. 4.** Graphene mode-locked EDFL that delivers 24 fs pulses [125]. (a) Laser configuration; (b) optical spectrum; (c) autocorrelation trace; (d) measured RF spectrum. Reproduced with permission. Copyright 2016, IOP Publishing.

**Table 3.    UFLs Mode-Locked by 2D Materials with High Repetition Rates**

| Laser Configuration | SA | Repetition Rate | Ref. |
|---|---|---|---|
| ~1 cm short linear-cavity EDFL | LPE-prepared graphene | 9.67 GHz | [134] |
| 21st-harmonic mode-locked ring-cavity EDFL | ME-prepared multilayer graphene | 2.22 GHz | [135] |
| Ring-cavity EDFL with FP filter | LPE-prepared graphene | 100 GHz | [136] |
| Ring-cavity EDFL with microfiber knot filter | LPE-prepared graphene | 106.7 GHz | [137] |
| Ring-cavity YDFL with microfiber knot filter | LPE-prepared graphene | 162 GHz | [137] |
| 418th-harmonic mode-locked ring-cavity EDFL | LPE-prepared TI – $Bi_2Te_3$ | 2.04 GHz | [138] |
| 170th-harmonic mode-locked ring-cavity EDFL | PLD-locked TI – $Bi_2Te_3$ | 2.95 GHz | [77] |
| ~22 cm short linear-cavity EDFL | LPE-prepared TMD – $MoS_2$ | 463 MHz | [139] |
| 212th-harmonic mode-locked ring-cavity EDFL | LPE-prepared TMD – $MoSe_2$ | 3.27 GHz | [140] |
| 10th-harmonic mode-locked ring-cavity HDFL | LPE-prepared BP | 290 MHz | [141] |
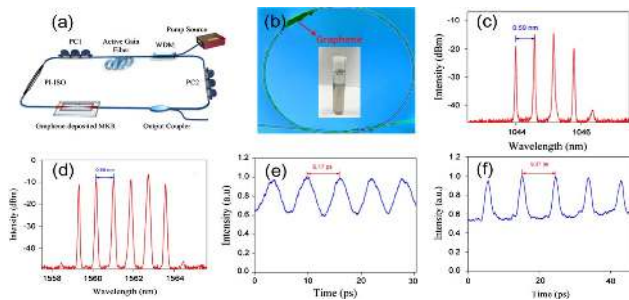


**Fig. 5.**    Hundred gigahertz repetition rate graphene mode-locked UFLs [137]. (a) Laser configuration; (b) graphene microfiber knot filter; (c) laser spectrum at 1 μm; (d) laser spectrum at 1.5 μm; (e) autocorrelation trace at 1 μm; (f) autocorrelation trace at 1.5 μm. Reproduced with permission. Copyright 2018, OSA Publishing.

Figure 5 shows a recent work by Liu *et al.* in which a graphene-deposited microfiber knot filter was used in ring-cavity fiber lasers, providing the spectral filtering and saturable absorption effect [137]. When the filter was implemented into a YDFL, a pulse train at 1 μm with a 162 GHz repetition rate was generated. When it was inserted into an EDFL, a pulse train in the 1.5 μm region with a 106.7 GHz repetition rate was addressed.

The harmonic mode-locking technique is an alternative important approach to realize high repetition rate outputs. In 2012, a graphene-based 21st-harmonic mode-locked fiber laser was reported by Sobon *et al.*, with a pulse repetition rate of 2.22 GHz [135]. Other kinds of 2D materials like TIs, TMDs, and BP are also efficient for achieving harmonic mode-locking operations. With a TI – $Bi_2Te_3$ fiber SA implemented in a ring-cavity EDFL, Luo *et al.* raised the repetition rate to

2.04 GHz, corresponding to a high harmonic order of 418 [138]. Another work by Yan *et al.* also utilized a TI – $Bi_2Se_3$ fiber SA in a ring-cavity EDFL, but with a higher fundamental repetition rate of 200 MHz. In this case, a harmonic mode-locking repetition rate of 2.95 GHz was obtained at a 170th-harmonic order [77]. To date, the highest repetition rate of a TMD mode-locked UFL was accomplished by Koo *et al.* in 2016 [140]. In their work, a $MoSe_2$/PVA composite depositing side-polished fiber was incorporated as an SA within a ring-cavity EDFL, where a repetition rate up to 3.27 GHz at a harmonic order of 212 was obtained. Considering various applications of high repetition rate pulses, we anticipate that high repetition rate UFLs mode-locked by 2D materials will continue to be a hot topic in the future.

### C. High Stability
Many applications of UFLs, such as optical frequency combs [142,143] and pure microwave generation, are in great need of highly stable ultralow-noise laser pulses. Therefore, the stability of a UFL is always the first consideration. A simple measurement to reflect the stability is to check the RF spectrum of pulse trains. If a mode-locked fiber laser has a high stability with RF harmonics extending to several gigahertz, it is regarded as an ideal device for gigahertz signal generation. Some representative results of UFLs mode-locked by 2D materials are summarized in Table 4.

In 2010, Popa *et al.* demonstrated a highly stable graphene mode-locked EDFL [120]. The ring-cavity laser had a net dispersion of $-0.052$ ps$^2$. A large RF signal-to-noise ratio (SNR) of 87.4 dB was realized at the fundamental repetition rate of 27.4 MHz. In 2014, Sobon *et al.* reported a high-power fiber CPA laser system at 1560 nm [144]. A highly stable CVD-grown graphene mode-locked EDFL was selected to provide seed pulses. It had an RF SNR of 70 dB at the repetition

**Table 4.    Highly Stable UFLs Mode-Locked by 2D Materials**

| Laser Configuration | SA | SNR at $f_{rep}$ | RF Resolution | RF Spanning | Ref. |
|---|---|---|---|---|---|
| Ring-cavity EDFL | LPE-prepared graphene | 87.4 dB | 10 Hz | – | [120] |
| Ring-cavity EDFL | CVD-grown graphene | 70 dB | – | 0–10 GHz | [144] |
| Ring-cavity TDFL | CVD-grown graphene | 75 dB | 33 Hz | 0–3.6 GHz | [126] |
| Ring-cavity EDFL | PMS-deposited TI – $In_2Se_3$ | 90 dB | 30 Hz | 0–1.5 GHz | [145] |
| Ring-cavity EDFL | PMS-deposited TMD – $MoTe_2$ | 93 dB | 10 Hz | 0–1 GHz | [146] |
| Ring-cavity TDFL | PMS-deposited TI – $Sb_2Te_3$ | 84 dB | 10 Hz | 0–1 GHz | [147] |
| Ring-cavity TDFL | PMS-deposited TI – $Wte_2$ | 95 dB | 10 Hz | 0–0.5 GHz | [148] |
| Ring-cavity EDFL | CVD-grown TMD – $WSe_2$ | 96 dB | 20 Hz | 0–0.6 GHz | [128] |
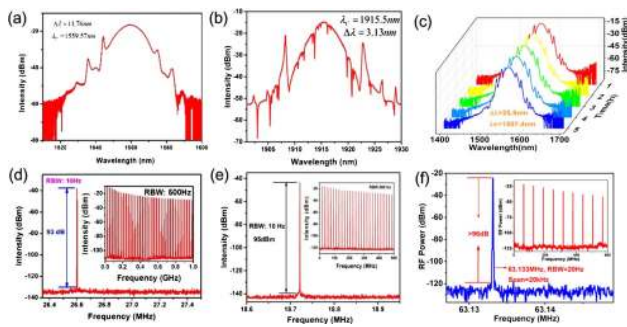
**Fig. 6.** Highly stable UFLs mode-locked by 2D materials. (a)–(c) Laser spectra; (d)–(f) measured RF spectra. (a) and (d), Ref. [146]; reproduced with permission; copyright 2018, OSA Publishing. (b) and (e), Ref. [148]; reproduced with permission; copyright 2017, OSA Publishing. (c) and (f), Ref. [128]; reproduced with permission; copyright 2018, IOP Publishing.

rate of 50 MHz, whose RF spectrum exhibits a slight decay compared to the case of 0–10 GHz, implying its high stability. Other 2D materials like TIs and TMDs have also been used for generating low-noise mode-locked UFLs. Yan *et al.* used the PMS technique to deposit TI and TMD films onto fiber tapers for fabricating high-performance fiber SAs. By inserting these fiber SAs into ring-cavity EDFLs [145,146] and TDFLs [147], stable mode-locked pulse trains with ultrahigh SNRs on RF spectra were obtained. In 2018, Liu *et al.* prepared a CVD-grown TMD-WSe$_2$ film and transferred it onto a tapered fiber to fabricate a fiber SA. They demonstrated a highest SNR of 96 dB at a pulse repetition rate of 63.133 MHz with a ring-cavity EDFL [146].

Figure 6 depicts the measured optical spectra and RF spectra of these representative results. As can be seen from the optical spectra, these highly stable laser pulses were all typical soliton pulses mode-locked in anomalous regimes. To further characterize the stabilities of mode-locked UFLs, relative intensity noise and time jittering should be taken into account. In the future, we hope that more techniques and methods will be used to suppress lasing noise and enhance long-term stability.

## 5. CHALLENGES AND FUTURE DIRECTIONS

According to previous discussions, there are indeed some aspects of 2D materials that are better than those of SESAMs, like excellent broadband saturable absorption and ultrashort recovery time. However, despite the current achievements, the lack of fine-controlled material fabrication still remains a hurdle to mass production of most of these 2D materials [133]. Maybe the industrialization of graphene is a great start. Besides, the long-term stability of these 2D materials should also be further exploited. Methods used for oxidation resistance [2], hydrolytic resistance [61], and suppression of photon-induced degradation should be fully considered as the next steps. We also think that the fabrication of a 2D material fiber SA with customized nonsaturable loss, modulation depth, and recovery time is of critical importance. It is likely that future work in this field will establish more systematic guidelines for SA design and optimization.

Obviously, there is abundant room for further progress in the pursuit of high-performance UFLs mode-locked by 2D materials. The broadband saturable absorption of 2D materials makes them good candidates for two-band mode-locking operations simultaneously. In 2014, Sotor *et al.* reported a passive synchronization of an EDFL and a TDFL enhanced by a common graphene SA [149]. It might help for few-cycle pulse generation with coherent combination or difference frequency generation in the mid-IR [150]. Meanwhile, the introduction of advanced optical techniques, such as time-lens [151], dispersive Fourier transform [152–154], and coherent sampling [155] measurements, to reveal the real-time pulse build-up dynamics of UFLs mode-locked by 2D materials is highly desirable. We believe that after getting insight into the buildup dynamics and making positive modifications to 2D materials-based SAs, many more high-performance UFLs will be put forward in the future. Although the main aim of this paper is to review the progress of UFLs mode-locked by 2D materials, we would like to point out the broadband 2D materials could also be exploited for novel photonic components, like photodetectors [156–160], sensors [161–164], active-optical modulators [165,166], and all-optical modulators [65,167–175]. Besides these, we also have confidence that more unprecedented ultralow-noise ultrafast mode-locked pulses or optical frequency combs will be realized with novel 2D materials-based SAs.

## 6. CONCLUSIONS

We have reviewed both initial and significant UFLs mode-locked by 2D materials in this paper. The intention of this review is to provide a brief survey of UFLs mode-locked by 2D materials in the past decade. Though it is not yet possible to be completely exhaustive, a number of important results have been covered, and future insights and challenges have been put forward.

†These authors contributed equally to this work.

## REFERENCES

1. U. Keller, K. J. Weingarten, F. X. Kartner, D. Kopf, B. Braun, I. D. Jung, R. Fluck, C. Honninger, N. Matuschek, and J. Aus der Au, "Semiconductor saturable absorber mirrors (SESAM's) for femtosecond to nanosecond pulse generation in solid-state lasers," IEEE J. Sel. Top. Quantum Electron. **2**, 435–453 (1996).

2. X. Liu, Q. Guo, and J. Qiu, "Emerging low-dimensional materials for nonlinear optics and ultrafast photonics," Adv. Funct. Mater. **29**, 1605886 (2017).

3. F. Wang, "Two-dimensional materials for ultrafast lasers," Chin. Phys. B **26**, 034202 (2017).

4. T. Jiang, R. Miao, J. Zhao, Z. Xu, T. Zhou, K. Wei, J. You, X. Zheng, Z. Wang, and X. A. Cheng, "Electron-phonon coupling in topological insulator $Bi_2Se_3$ thin films with different substrates," Chin. Opt. Lett. **17**, 020005 (2019).

5. L. Miao, J. Yi, Q. Wang, D. Feng, H. He, S. Lu, C. Zhao, H. Zhang, and S. Wen, "Broadband third order nonlinear optical responses of bismuth telluride nanosheets," Opt. Mater. Express **6**, 2244–2251 (2016).

6. Z. Guo, S. Chen, Z. Wang, Z. Yang, F. Liu, Y. Xu, J. Wang, Y. Yi, H. Zhang, L. Liao, P. K. Chu, and X. F. Yu, "Metal-ion-modified black phosphorus with enhanced stability and transistor performance," Adv. Mater. **29**, 1703811 (2017).

7. T. Fan, Y. Zhou, M. Qiu, and H. Zhang, "Black phosphorus: a novel nanoplatform with potential in the field of bio-photonic nanomedicine," J. Innov. Opt. Heal. Sci. **11**, 1830003 (2018).

8. X. Chen, G. Xu, X. Ren, Z. Li, X. Qi, K. Huang, H. Zhang, Z. Huang, and J. Zhong, "A black/red phosphorus hybrid as an electrode material for high-performance Li-ion batteries and supercapacitors," J. Mater. Chem. A **5**, 6581–6588 (2017).

9. Q. Jiang, L. Xu, N. Chen, H. Zhang, L. Dai, and S. Wang, "Facile synthesis of black phosphorus: an efficient electrocatalyst for the oxygen evolving reaction," Angew. Chem. (Int. Ed. Engl.) **55**, 13849–13853 (2016).

10. Q. Bao, H. Zhang, Y. Wang, Z. Ni, Y. Yan, Z. X. Shen, K. P. Loh, and D. Y. Tang, "Atomic-layer graphene as a saturable absorber for ultrafast pulsed lasers," Adv. Funct. Mater. **19**, 3077–3083 (2009).

11. H. Yu, X. Zheng, K. Yin, X. A. Cheng, and T. Jiang, "Nanosecond passively Q-switched thulium/holmium-doped fiber laser based on black phosphorus nanoplatelets," Opt. Mater. Express **6**, 603–609 (2016).

12. Z. Sun, T. Hasan, F. Torrisi, D. Popa, G. Privitera, F. Wang, F. Bonaccorso, D. M. Basko, and A. C. Ferrari, "Graphene mode-locked ultrafast laser," ACS Nano **4**, 803–810 (2010).

13. K. S. Novoselov, A. K. Geim, S. V. Morozov, D. Jiang, M. I. Katsnelson, I. V. Grigorieva, S. V. Dubonos, and A. A. Firsov, "Two-dimensional gas of massless Dirac fermions in graphene," Nature **438**, 197–200 (2005).

14. A. K. Geim and K. S. Novoselov, "The rise of graphene," Nat. Mater. **6**, 183–191 (2007).

15. J. E. Moore, "The birth of topological insulators," Nature **464**, 194–198 (2010).

16. H. Zhang, C. Liu, X. Qi, X. Dai, Z. Fang, and S. Zhang, "Topological insulators in $Bi_2Se_3$, $Bi_2Te_3$ and $Sb_2Te_3$ with a single Dirac cone on the surface," Nat. Phys. **5**, 438–442 (2009).

17. K. F. Mak and J. Shan, "Photonics and optoelectronics of 2D semiconductor transition metal dichalcogenides," Nat. Photonics **10**, 216–226 (2016).

18. A. J. Fleisher, D. A. Long, Z. D. Reed, J. T. Hodges, and D. F. Plusquellic, "Coherent cavity-enhanced dual-comb spectroscopy," Opt. Express **24**, 10424–10434 (2016).

19. F. Xia, H. Wang, and Y. Jia, "Rediscovering black phosphorus as an anisotropic layered material for optoelectronics and electronics," Nat. Commun. **5**, 4458 (2014).

20. M. Buscema, D. J. Groenendijk, S. I. Blanter, G. A. Steele, H. S. van der Zant, and A. Castellanos-Gomez, "Fast and broadband photoresponse of few-layer black phosphorus field-effect transistors," Nano Lett. **14**, 3347–3352 (2014).

21. Y. Dong, S. Chertopalov, K. Maleski, B. Anasori, L. Hu, S. Bhattacharya, A. M. Rao, Y. Gogotsi, V. N. Mochalin, and R. Podila, "Saturable absorption in 2D $Ti_3C_2$ MXene thin films for passive photonic diodes," Adv. Optical Mater. **30**, 1705714 (2018).

22. M. Naguib, V. N. Mochalin, M. W. Barsoum, and Y. Gogotsi, "25th anniversary article: Mxenes: a new family of two-dimensional materials," Adv. Funct. Mater. **26**, 992–1005 (2014).

23. E. Aktürk, O. Ü. Aktürk, and S. Ciraci, "Single and bilayer bismuthene: stability at high temperature and mechanical and electronic properties," Phys. Rev. B **94**, 014115 (2016).

24. M. Pumera and Z. Sofer, "2D monoelemental arsenene, antimonene, and bismuthene: beyond black phosphorus," Adv. Mater. **29**, 1605299 (2017).

25. S. Yamashita, A. Martinez, and B. Xu, "Short pulse fiber lasers mode-locked by carbon nanotubes and graphene," Opt. Fiber Technol. **20**, 702–713 (2014).

26. G. Soboń, "Mode-locking of fiber lasers using novel two-dimensional nanomaterials: graphene and topological insulators [invited]," Photon. Res. **3**, A56–A63 (2015).

27. Z. C. Luo, M. Liu, A. P. Luo, and W. C. Xu, "Two-dimensional materials-decorated microfiber devices for pulse generation and shaping in fiber lasers," Chin. Phys. B **27**, 094215 (2018).

28. K. Wu, B. Chen, X. Zhang, S. Zhang, C. Guo, C. Li, P. Xiao, J. Wang, L. Zhou, W. Zou, and J. Chen, "High-performance mode-locked and Q-switched fiber lasers based on novel 2D materials of topological insulators, transition metal dichalcogenides and black phosphorus: review and perspective (invited)," Opt. Commun. **406**, 214–229 (2018).

29. J. He, L. Tao, H. Zhang, B. Zhou, and J. Li, "Emerging 2D materials beyond graphene for ultrashort pulse generation in fiber lasers," Nanoscale **11**, 2577–2593 (2019).

30. B. Fu, Y. Hua, X. Xiao, H. Zhu, Z. Sun, and C. Yang, "Broadband graphene saturable absorber for pulsed fiber lasers at 1, 1.5, and 2 μm," IEEE J. Sel. Top. Quantum Electron. **20**, 1100705 (2014).

31. Y. Jiang, L. Miao, G. Jiang, Y. Chen, X. Qi, X. Jiang, H. Zhang, and S. Wen, "Broadband and enhanced nonlinear optical response of $MoS_2$/graphene nanocomposites for ultrafast photonics applications," Sci. Rep. **5**, 16372 (2015).

32. L. Kong, Z. Qin, G. Xie, Z. Guo, H. Zhang, P. Yuan, and L. Qian, "Black phosphorus as broadband saturable absorber for pulsed lasers from 1 μm to 2.7 μm wavelength," Laser Phys. Lett. **13**, 045801 (2016).

33. Y.-W. Song, S.-Y. Jang, W.-S. Han, and M.-K. Bae, "Graphene mode-lockers for fiber lasers functioned with evanescent field interaction," Appl. Phys. Lett. **96**, 051122 (2010).

34. S. Yamashita, "A tutorial on nonlinear photonic applications of carbon nanotube and graphene," J. Lightwave Technol. **30**, 427–447 (2012).

35. H. Zhang, X. He, W. Lin, R. Wei, F. Zhang, X. Du, G. Dong, and J. Qiu, "Ultrafast saturable absorption in topological insulator $Bi_2SeTe_2$ nanosheets," Opt. Express **23**, 13376–13383 (2015).

36. H. Zhang, S. Virally, Q. Bao, L. Kian Ping, S. Massar, N. Godbout, and P. Kockaert, "Z-scan measurement of the nonlinear refractive index of graphene," Opt. Lett. **37**, 1856–1858 (2012).

37. X. Zheng, Y. Zhang, R. Chen, X. A. Cheng, Z. Xu, and T. Jiang, "Z-scan measurement of the nonlinear refractive index of monolayer $WS_2$," Opt. Express **23**, 15616–15623 (2015).

38. G. Wang, K. Wang, B. M. Szydłowska, A. A. Baker-Murray, J. J. Wang, Y. Feng, X. Zhang, J. Wang, and W. J. Blau, "Ultrafast nonlinear optical properties of a graphene saturable mirror in the 2 μm wavelength region," Laser Photon. Rev. **11**, 1700166 (2017).

39. P. Miró, M. Audiffred, and T. Heine, "An atlas of two-dimensional materials," Chem. Soc. Rev. **43**, 6537–6554 (2014).

40. K. J. Koski, C. D. Wessells, B. W. Reed, J. J. Cha, D. Kong, and Y. Cui, "Chemical intercalation of zerovalent metals into 2D layered $Bi_2Se_3$ nanoribbons," J. Am. Chem. Soc. **134**, 13773–13779 (2012).

41. J. Zhao, Z. Xu, Y. Zang, Y. Gong, X. Zheng, K. He, X. A. Cheng, and T. Jiang, "Thickness-dependent carrier and phonon dynamics of topological insulator $Bi_2Te_3$ thin films," Opt. Express **25**, 14635–14643 (2017).

42. A. Splendiani, L. Sun, Y. Zhang, T. Li, J. Kim, C. Y. Chim, G. Galli, and F. Wang, "Emerging photoluminescence in monolayer $MoS_2$," Nano Lett. **10**, 1271–1275 (2010).

43. M. Xu, T. Liang, M. Shi, and H. Chen, "Graphene-like two-dimensional materials," Chem. Rev. **113**, 3766–3798 (2013).

44. S. Lu and J. Leburton, "Electronic structures of defects and magnetic impurities in $MoS_2$ monolayers," Nanoscale Res. Lett. **9**, 676 (2014).

45. V. Tran, R. Soklaski, Y. Liang, and L. Yang, "Layer-controlled band gap and anisotropic excitons in few-layer black phosphorus," Phys. Rev. B **89**, 235319 (2014).

46. V. Tran, R. Fei, and L. Yang, "Quasiparticle energies, excitons, and optical spectra of few-layer black phosphorus," 2D Mater. **2**, 044014 (2015).

47. Y. I. Jhon, J. Koo, B. Anasori, M. Seo, J. H. Lee, Y. Gogotsi, and Y. M. Jhon, "Metallic MXene saturable absorber for femtosecond mode-locked lasers," Adv. Funct. Mater. **29**, 1702496 (2017).

48. M.-Y. Liu, Y. Huang, Q.-Y. Chen, Z.-Y. Li, C. Cao, and Y. He, "Strain and electric field tunable electronic structure of buckled bismuthene," RSC Adv. **7**, 39546–39555 (2017).

49. Q.-Q. Yang, R.-T. Liu, C. Huang, Y.-F. Huang, L.-F. Gao, B. Sun, Z.-P. Huang, L. Zhang, C.-X. Hu, Z.-Q. Zhang, C.-L. Sun, Q. Wang, Y.-L. Tang, and H.-L. Zhang, "2D bismuthene fabricated via acid-intercalated exfoliation showing strong nonlinear near-infrared responses for mode-locking lasers," Nanoscale **10**, 21106–21115 (2018).

50. M. Z. Hasan and C. L. Kane, "Colloquium: topological insulators," Rev. Mod. Phys. **82**, 3045–3067 (2010).

51. M. Chhowalla, H. S. Shin, G. Eda, L.-J. Li, K. P. Loh, and H. Zhang, "The chemistry of two-dimensional layered transition metal dichalcogenide nanosheets," Nat. Chem. **5**, 263–275 (2013).

52. M. M. Ugeda, A. J. Bradley, S.-F. Shi, F. H. da Jornada, Y. Zhang, D. Y. Qiu, W. Ruan, S.-K. Mo, Z. Hussain, Z.-X. Shen, F. Wang, S. G. Louie, and M. F. Crommie, "Giant bandgap renormalization and excitonic effects in a monolayer transition metal dichalcogenide semiconductor," Nat. Mater. **13**, 1091–1095 (2014).

53. J. Lee, J. Koo, J. Lee, Y. M. Jhon, and J. H. Lee, "All-fiberized, femtosecond laser at 1912 nm using a bulk-like MoSe₂ saturable absorber," Opt. Mater. Express **7**, 2968–2979 (2017).

54. Y. Cui, F. Lu, and X. Liu, "Nonlinear saturable and polarization-induced absorption of rhenium disulfide," Sci. Rep. **7**, 40080 (2017).

55. A. Castellanos-Gomez, L. Vicarelli, E. Prada, J. O. Island, K. L. Narasimha-Acharya, S. I. Blanter, D. J. Groenendijk, M. Buscema, G. A. Steele, J. V. Alvarez, H. W. Zandbergen, J. J. Palacios, and H. S. J. van der Zant, "Isolation and characterization of few-layer black phosphorus," 2D Mater. **1**, 025001 (2014).

56. J. Sotor, G. Soboń, W. Macherzynski, P. Paletko, and K. M. Abramski, "Black phosphorus saturable absorber for ultrashort pulse generation," Appl. Phys. Lett. **107**, 051108 (2015).

57. L. Li, Y. Yu, G. J. Ye, Q. Ge, X. Ou, H. Wu, D. Feng, X. H. Chen, and Y. Zhang, "Black phosphorus field-effect transistors," Nat. Nano **9**, 372–377 (2014).

58. J. Du, M. Zhang, Z. Guo, J. Chen, X. Zhu, G. Hu, P. Peng, Z. Zheng, and H. Zhang, "Phosphorene quantum dot saturable absorbers for ultrafast fiber lasers," Sci. Rep. **7**, 42357 (2017).

59. J. Liu, J. Liu, Z. Guo, H. Zhang, W. Ma, J. Wang, and L. Su, "Dual-wavelength Q-switched Er:SrF₂ laser with a black phosphorus absorber in the mid-infrared region," Opt. Express **24**, 30289–30295 (2016).

60. K. Wang, B. M. Szydlowska, G. Wang, X. Zhang, J. J. Wang, J. J. Magan, L. Zhang, J. N. Coleman, J. Wang, and W. J. Blau, "Ultrafast nonlinear excitation dynamics of black phosphorus nanosheets from visible to mid-infrared," ACS Nano **10**, 6923–6932 (2016).

61. D. Na, K. Park, K.-H. Park, and Y.-W. Song, "Passivation of black phosphorus saturable absorbers for reliable pulse formation of fiber lasers," Nanotechnology **28**, 475207 (2017).

62. M. Naguib, J. Come, B. Dyatkin, V. Presser, P.-L. Taberna, P. Simon, M. W. Barsoum, and Y. Gogotsi, "MXene: a promising transition metal carbide anode for lithium-ion batteries," Electrochem. Commun. **16**, 61–64 (2012).

63. P. Li, Y. Chen, T. Yang, Z. Wang, H. Lin, Y. Xu, L. Li, H. Mu, B. N. Shivananju, Y. Zhang, Q. Zhang, A. Pan, S. Li, D. Tang, B. Jia, H. Zhang, and Q. Bao, "Two-dimensional CH₃NH₃PbI₃ perovskite nanosheets for ultrafast pulsed fiber lasers," ACS Appl. Mater. Interfaces **9**, 12759–12765 (2017).

64. Z. Liu, H. Mu, S. Xiao, R. Wang, Z. Wang, W. Wang, Y. Wang, X. Zhu, K. Lu, H. Zhang, S. T. Lee, Q. Bao, and W. Ma, "Pulsed lasers employing solution-processed plasmonic Cu₃₋ₓP colloidal nanocrystals," Adv. Mater. **28**, 3535–3542 (2016).

65. Y. Song, Z. Liang, X. Jiang, Y. Chen, Z. Li, L. Lu, Y. Ge, K. Wang, J. Zheng, S. Lu, J. Ji, and H. Zhang, "Few-layer antimonene decorated microfiber: ultra-short pulse generation and all-optical thresholding with enhanced long term stability," 2D Mater. **4**, 045010 (2017).

66. R. Frisenda, E. Navarro-Moratalla, P. Gant, D. Perez De Lara, P. Jarillo-Herrero, R. V. Gorbachev, and A. Castellanos-Gomez, "Recent progress in the assembly of nanodevices and van der Waals heterostructures by deterministic placement of 2D materials," Chem. Soc. Rev. **47**, 53–68 (2018).

67. Y. Wang, H. Mu, X. Li, J. Yuan, J. Chen, S. Xiao, Q. Bao, Y. Gao, and J. He, "Observation of large nonlinear responses in a graphene-Bi₂Te₃ heterostructure at a telecommunication wavelength," Appl. Phys. Lett. **108**, 221901 (2016).

68. H. Mu, Z. Wang, J. Yuan, S. Xiao, C. Chen, Y. Chen, Y. Chen, J. Song, Y. Wang, Y. Xue, H. Zhang, and Q. Bao, "Graphene-Bi₂Te₃ heterostructure as saturable absorber for short pulse generation," ACS Photon. **2**, 832–841 (2015).

69. W. Liu, Y.-N. Zhu, M. Liu, B. Wen, S. Fang, H. Teng, M. Lei, L.-M. Liu, and Z. Wei, "Optical properties and applications for MoS₂-Sb₂Te₃-MoS₂ heterostructure materials," Photon. Res. **6**, 220–227 (2018).

70. Z. Wang, H. Mu, J. Yuan, C. Zhao, Q. Bao, and H. Zhang, "Graphene-Bi₂Te₃ heterostructure as broadband saturable absorber for ultra-short pulse generation in Er-doped and Yb-doped fiber lasers," IEEE J. Sel. Top. Quantum Electron. **23**, 8800105 (2016).

71. H. Chen, J. Yin, J. Yang, X. Zhang, M. Liu, Z. Jiang, J. Wang, Z. Sun, T. Guo, W. Liu, and P. Yan, "Transition-metal dichalcogenides heterostructure saturable absorbers for ultrafast photonics," Opt. Lett. **42**, 4279–4282 (2017).

72. B. G. B. Guo, "2D noncarbon materials-based nonlinear optical devices for ultrafast photonics [invited]," Chin. Opt. Lett. **16**, 020004 (2018).

73. Y. M. Chang, H. Kim, J. H. Lee, and Y.-W. Song, "Multilayered graphene efficiently formed by mechanical exfoliation for nonlinear saturable absorbers in fiber mode-locked lasers," Appl. Phys. Lett. **97**, 211102 (2010).

74. K. Wang, J. Wang, J. Fan, M. Lotya, A. O'Neill, D. Fox, Y. Feng, X. Zhang, B. Jiang, Q. Zhao, H. Zhang, J. N. Coleman, L. Zhang, and W. J. Blau, "Ultrafast saturable absorption of two-dimensional MoS₂ nanosheets," ACS Nano **7**, 9260–9267 (2013).

75. X. Zhang and Y. Xie, "Recent advances in free-standing two-dimensional crystals with atomic thickness: design, assembly and transfer strategies," Chem. Soc. Rev. **42**, 8187–8199 (2013).

76. C. Y. Yeh, C. Y. Su, G. R. Lin, H. H. Kuo, L. J. Li, P. L. Huang, S. C. Lin, S. H. Huang, and W. H. Cheng, "Stable mode-locked fiber laser based on CVD fabricated graphene saturable absorber," Opt. Express **20**, 2460–2465 (2012).

77. P. Yan, R. Lin, S. Ruan, A. Liu, and H. Chen, "A 2.95 GHz, femtosecond passive harmonic mode-locked fiber laser based on evanescent field interaction with topological insulator film," Opt. Express **23**, 154–164 (2015).

78. M. Kowalczyk, J. Bogusławski, R. Zybała, K. Mars, A. Mikuła, G. Soboń, and J. Sotor, "Sb₂Te₃-deposited D-shaped fiber as a saturable absorber for mode-locked Yb-doped fiber lasers," Opt. Mater. Express **6**, 2273–2282 (2016).

79. L. Miao, Y. Jiang, S. Lu, B. Shi, C. Zhao, H. Zhang, and S. Wen, "Broadband ultrafast nonlinear optical response of few-layers graphene: toward the mid-infrared regime," Photon. Res. **3**, 214–219 (2015).

80. H. Hao, Z. Xu, T. Jiang, K. Wei, H. Li, X. Zheng, K. Yin, J. You, C. Shen, and X. A. Cheng, "Visualized charge transfer processes in monolayer composition-graded WS₂ₓSe₂₍₁₋ₓ₎ lateral heterojunctions via ultrafast microscopy mapping," Opt. Express **26**, 15867–15886 (2018).

81. M. C. Fischer, J. W. Wilson, F. E. Robles, and W. S. Warren, "Invited review article: pump-probe microscopy," Rev. Sci. Instrum. **87**, 031101 (2016).

82. A. Reina, H. B. Son, L. Y. Jiao, B. Fan, M. S. Dresselhaus, Z. F. Liu, and J. Kong, "Transferring and identification of single- and few-layer graphene on arbitrary substrates," J. Phys. Chem. C **112**, 17741–17744 (2008).

83. T. Chen, C. Liao, D. N. Wang, and Y. Wang, "Polarization-locked vector solitons in a mode-locked fiber laser using polarization-sensitive few-layer graphene deposited D-shaped fiber saturable absorber," J. Opt. Soc. Am. B **31**, 1377–1382 (2014).

84. X. Liu, H. Yang, Y. Cui, G. Chen, Y. Yang, X. Wu, X. Yao, D. Han, X. Han, and C. Zeng, "Graphene-clad microfibre saturable absorber for ultrafast fibre lasers," Sci. Rep. **6**, 26024 (2016).

85. D. Steinberg, J. Diego Zapata, E. A. Thoroh de Souza, and L. A. M. Saito, "Mechanically exfoliated graphite onto D-shaped optical fiber for femtosecond mode-locked erbium-doped fiber laser," J. Lightwave Technol. **36**, 1868–1874 (2018).

86. J. Zhao, S. Ruan, P. Yan, H. Zhang, Y. Yu, H. Wei, and J. Luo, "Cladding-filled graphene in a photonic crystal fiber as a saturable absorber and its first application for ultrafast all-fiber laser," Opt. Eng. **52**, 106105 (2013).

87. S. Ko, J. Lee, J. Koo, B. S. Joo, M. Gu, and J. H. Lee, "Chemical wet etching of an optical fiber using a hydrogen fluoride-free solution for a saturable absorber based on the evanescent field interaction," J. Lightwave Technol. **34**, 3776–3784 (2016).

88. H. Jeong, S. Y. Choi, F. Rotermund, Y.-H. Cha, D.-Y. Jeong, and D.-I. Yeom, "All-fiber mode-locked laser oscillator with pulse energy of 34 nJ using a single-walled carbon nanotube saturable absorber," Opt. Express **22**, 22667–22672 (2014).

89. L. Gao, T. Zhu, Y. J. Li, W. Huang, and M. Liu, "Watt-level ultrafast fiber laser based on weak evanescent interaction with reduced graphene oxide," IEEE Photon. Technol. Lett. **28**, 1245–1248 (2016).

90. D. Mao, S. Zhang, Y. Wang, X. Gan, W. Zhang, T. Mei, Y. Wang, Y. Wang, H. Zeng, and J. Zhao, "WS$_2$ saturable absorber for dissipative soliton mode locking at 1.06 and 1.55 μm," Opt. Express **23**, 27509–27519 (2015).

91. H. Shalibeik, _Rare-Earth-Doped Fiber Lasers and Amplifiers_ (Cuvillier Verlag, 2007).

92. W. Shi, Q. Fang, X. Zhu, R. A. Norwood, and N. Peyghambarian, "Fiber lasers and their applications [invited]," Appl. Opt. **53**, 6554–6568 (2014).

93. D. D. Hudson, "Invited paper: short pulse generation in mid-IR fiber lasers," Opt. Fiber Technol. **20**, 631–641 (2014).

94. F. Haxsen, A. Wienke, D. Wandt, J. Neumann, and D. Kracht, "Tm-doped mode-locked fiber lasers," Opt. Fiber Technol. **20**, 650–656 (2014).

95. H. Zhang, D. Y. Tang, L. M. Zhao, Q. L. Bao, and K. P. Loh, "Large energy mode locking of an erbium-doped fiber laser with atomic layer graphene," Opt. Express **17**, 17630–17635 (2009).

96. L. M. Zhao, D. Y. Tang, H. Zhang, X. Wu, Q. Bao, and K. P. Loh, "Dissipative soliton operation of an ytterbium-doped fiber laser mode locked with atomic multilayer graphene," Opt. Lett. **35**, 3622–3624 (2010).

97. M. Zhang, E. J. R. Kelleher, F. Torrisi, Z. Sun, T. Hasan, D. Popa, F. Wang, A. C. Ferrari, S. V. Popov, and J. R. Taylor, "Tm-doped fiber laser mode-locked by graphene-polymer composite," Opt. Express **20**, 25077–25084 (2012).

98. N. T. V. Dvoyrin, E. Sorokin, I. Sorokina, and A. Kurkov, "Graphene-mode-locked Holmium fiber laser operating beyond 2.1 μm," in _European Conference on Lasers and Electro-Optics—European Quantum Electronics Conference_, Munich, Germany (2015), paper CJ_7_4.

99. C. Zhao, H. Zhang, X. Qi, Y. Chen, Z. Wang, S. Wen, and D. Tang, "Ultra-short pulse generation by a topological insulator based saturable absorber," Appl. Phys. Lett. **101**, 211106 (2012).

100. H. Zhang, S. B. Lu, J. Zheng, J. Du, S. C. Wen, D. Y. Tang, and K. P. Loh, "Molybdenum disulfide (MoS$_2$) as a broadband saturable absorber for ultra-fast photonics," Opt. Express **22**, 7249–7260 (2014).

101. Y. Chen, G. Jiang, S. Chen, Z. Guo, X. Yu, C. Zhao, H. Zhang, Q. Bao, S. Wen, D. Tang, and D. Fan, "Mechanically exfoliated black phosphorus as a new saturable absorber for both Q-switching and Mode-locking laser operation," Opt. Express **23**, 12823–12833 (2015).

102. L. Lu, Z. Liang, L. Wu, Y. Chen, Y. Song, S. C. Dhanabalan, J. S. Ponraj, B. Dong, Y. Xiang, F. Xing, D. Fan, and H. Zhang, "Few-layer bismuthene: sonochemical exfoliation, nonlinear optics and applica-

tions for ultrafast photonics with enhanced stability," Laser Photon. Rev. **12**, 1700221 (2018).

103. Z. Dou, Y. Song, J. Tian, J. Liu, Z. Yu, and X. Fang, "Mode-locked ytterbium-doped fiber laser based on topological insulator: Bi$_2$Se$_3$," Opt. Express **22**, 24055–24061 (2014).

104. M. Jung, J. Lee, J. Koo, J. Park, Y. Song, K. Lee, S. Lee, and J. H. Lee, "A femtosecond pulse fiber laser at 1935 nm using a bulk-structured Bi$_2$Te$_3$ topological insulator," Opt. Express **22**, 7865–7874 (2014).

105. H. Liu, A.-P. Luo, F.-Z. Wang, R. Tang, M. Liu, Z.-C. Luo, W.-C. Xu, C.-J. Zhao, and H. Zhang, "Femtosecond pulse erbium-doped fiber laser by a few-layer MoS$_2$ saturable absorber," Opt. Lett. **39**, 4591–4594 (2014).

106. M. Jung, J. Lee, J. Park, J. Koo, Y. M. Jhon, and J. H. Lee, "Mode-locked, 1.94-μm, all-fiberized laser using WS$_2$-based evanescent field interaction," Opt. Express **23**, 19996–20006 (2015).

107. A. A. Latiff, M. F. M. Rusdi, M. B. Hisyam, H. Ahmad, and S. W. Harun, "Black phosphorus as a saturable absorber for generating mode-locked fiber laser in normal dispersion regime," Proc. SPIE **10150**, 101500U (2016).

108. J. Sotor, G. Soboń, M. Kowalczyk, W. Macherzynski, P. Paletko, and K. M. Abramski, "Ultrafast thulium-doped fiber laser mode locked with black phosphorus," Opt. Lett. **40**, 3885–3888 (2015).

109. K. Yin, T. Jiang, X. Zheng, H. Yu, X. Cheng, and J. Hou, "Mid-infrared ultra-short mode-locked fiber laser utilizing topological insulator Bi$_2$Te$_3$ nano-sheets as the saturable absorber," arXiv:1505.06322 (2015).

110. G. Zhu, X. Zhu, F. Wang, S. Xu, Y. Li, X. Guo, K. Balakrishnan, R. A. Norwood, and N. Peyghambarian, "Graphene mode-locked fiber laser at 2.8 μm," IEEE Photon. Technol. Lett. **28**, 7–10 (2016).

111. Z. Qin, G. Xie, C. Zhao, S. Wen, P. Yuan, and L. Qian, "Mid-infrared mode-locked pulse generation with multilayer black phosphorus as saturable absorber," Opt. Lett. **41**, 56–59 (2016).

112. Z. Qin, T. Hai, G. Xie, J. Ma, P. Yuan, L. Qian, L. Li, L. Zhao, and D. Shen, "Black phosphorus Q-switched and mode-locked mid-infrared Er:ZBLAN fiber laser at 3.5 μm wavelength," Opt. Express **26**, 8224–8231 (2018).

113. C. A. Schäfer, H. Uehara, D. Konishi, S. Hattori, H. Matsukuma, M. Murakami, S. Shimizu, and S. Tokita, "Fluoride-fiber-based side-pump coupler for high-power fiber lasers at 2.8 μm," Opt. Lett. **43**, 2340–2343 (2018).

114. N. Q. Ngo, _Ultra-Fast Fiber Lasers: Principles and Applications with MATLAB Models_ (CRC Press, 2011).

115. J. R. Taylor, _Optical Solitons: Theory and Experiment_ (Cambridge University, 1992).

116. J. Jeon, J. Lee, and J. H. Lee, "Numerical study on the minimum modulation depth of a saturable absorber for stable fiber laser mode locking," J. Opt. Soc. Am. B **32**, 31–37 (2014).

117. G. Soboń, J. Sotor, I. Pasternak, A. Krajewska, W. Strupinski, and K. M. Abramski, "Multilayer graphene-based saturable absorbers with scalable modulation depth for mode-locked Er- and Tm-doped fiber lasers," Opt. Mater. Express **5**, 2884–2894 (2015).

118. J. Zhang, T. Jiang, T. Zhou, H. Ouyang, C. Zhang, Z. Xin, Z. Wang, and X. A. Cheng, "Saturated absorption of different layered Bi$_2$Se$_3$ films in the resonance zone [invited]," Photon. Res. **6**, C8–C14 (2018).

119. H.-D. Xia, H.-P. Li, C.-Y. Lan, C. Li, G.-L. Deng, J.-F. Li, and Y. Liu, "Passive harmonic mode-locking of Er-doped fiber laser using CVD-grown few-layer MoS$_2$ as a saturable absorber," Chin. Phys. B **24**, 084206 (2015).

120. D. Popa, Z. Sun, F. Torrisi, T. Hasan, F. Wang, and A. C. Ferrari, "Sub 200 fs pulse generation from a graphene mode-locked fiber laser," Appl. Phys. Lett. **97**, 203106 (2010).

121. R. Lindberg, J. Bogusławski, I. Pasternak, A. Przewloka, F. Laurell, V. Pasiskevicius, and J. Sotor, "Mapping mode-locking regimes in a polarization-maintaining Er-doped fiber laser," IEEE J. Sel. Top. Quantum Electron. **24**, 1101709 (2018).

122. J. Sotor, I. Pasternak, A. Krajewska, W. Strupinski, and G. Soboń, "Sub-90 fs a stretched-pulse mode-locked fiber laser based on a graphene saturable absorber," Opt. Express **23**, 27503–27508 (2015).

123. G. Soboń, J. Sotor, I. Pasternak, A. Krajewska, W. Strupinski, and K. M. Abramski, "All-polarization maintaining, graphene-based femtosecond Tm-doped all-fiber laser," Opt. Express **23**, 9339–9346 (2015).

124. M. Pawliszewska, A. Przewloka, and J. Sotor, "Stretched-pulse Ho-doped fiber laser mode-locked by graphene based saturable absorber," Proc. SPIE **10512**, 105121A (2018).

125. J. Sotor and G. Soboń, "24 fs and 3 nJ pulse generation from a simple, all polarization maintaining Er-doped fiber laser," Laser Phys. Lett. **13**, 125102 (2016).

126. G. Soboń, J. Sotor, I. Pasternak, A. Krajewska, W. Strupinski, and K. M. Abramski, "260 fs and 1 nJ pulse generation from a compact, mode-locked Tm-doped fiber laser," Opt. Express **23**, 31446–31451 (2015).

127. W. Liu, L. Pang, H. Han, W. Tian, H. Chen, M. Lei, P. Yan, and Z. Wei, "70-fs mode-locked erbium-doped fiber laser with topological insulator," Sci. Rep. **6**, 19997 (2016).

128. W. Liu, M. Liu, Y. OuYang, H. Hou, G. Ma, M. Lei, and Z. Wei, "Tungsten diselenide for mode-locked erbium-doped fiber lasers with short pulse duration," Nanotechnology **29**, 174002 (2018).

129. W. Liu, L. Pang, H. Han, M. Liu, M. Lei, S. Fang, H. Teng, and Z. Wei, "Tungsten disulfide saturable absorbers for 67 fs mode-locked erbium-doped fiber lasers," Opt. Express **25**, 2950–2959 (2017).

130. X. Jin, G. Hu, M. Zhang, Y. Hu, T. Albrow-Owen, R. C. T. Howe, T. C. Wu, Q. Wu, Z. Zheng, and T. Hasan, "102 fs pulse generation from a long-term stable, inkjet-printed black phosphorus-mode-locked fiber laser," Opt. Express **26**, 12506–12513 (2018).

131. J. Li, H. Luo, B. Zhai, R. Lu, Z. Guo, H. Zhang, and Y. Liu, "Black phosphorus: a two-dimension saturable absorption material for mid-infrared Q-switched and mode-locked fiber lasers," Sci. Rep. **6**, 30361 (2016).

132. B. Guo, S. H. Wang, Z. X. Wu, Z. X. Wang, D. H. Wang, H. Huang, F. Zhang, Y. Q. Ge, and H. Zhang, "Sub-200 fs soliton mode-locked fiber laser based on bismuthene saturable absorber," Opt. Express **26**, 22750–22760 (2018).

133. X. Jiang, S. Liu, W. Liang, S. Luo, Z. He, Y. Ge, H. Wang, R. Cao, F. Zhang, Q. Wen, J. Li, Q. Bao, D. Fan, and H. Zhang, "Broadband nonlinear photonics in few-layer MXene Ti$_3$C$_2$T$_x$ (T = F, O, or OH)," Laser Photon. Rev. **12**, 1700229 (2018).

134. A. Martinez and S. Yamashita, "10 GHz fundamental mode fiber laser using a graphene saturable absorber," Appl. Phys. Lett. **101**, 041118 (2012).

135. G. Soboń, J. Sotor, and K. M. Abramski, "Passive harmonic mode-locking in Er-doped fiber laser based on graphene saturable absorber with repetition rates scalable to 2.22 GHz," Appl. Phys. Lett. **100**, 161109 (2012).

136. Y. L. Qi, H. Liu, H. Cui, Y. Q. Huang, Q. Y. Ning, M. Liu, Z. C. Luo, A. P. Luo, and W. C. Xu, "Graphene-deposited microfiber photonic device for ultrahigh-repetition rate pulse generation in a fiber laser," Opt. Express **23**, 17720–17726 (2015).

137. M. Liu, R. Tang, A.-P. Luo, W.-C. Xu, and Z.-C. Luo, "Graphene-decorated microfiber knot as a broadband resonator for ultrahigh repetition-rate pulse fiber lasers," Photon. Res. **6**, C1–C7 (2018).

138. Z. C. Luo, M. Liu, H. Liu, X. W. Zheng, A. P. Luo, C. J. Zhao, H. Zhang, S. C. Wen, and W. C. Xu, "2 GHz passively harmonic mode-locked fiber laser by a microfiber-based topological insulator saturable absorber," Opt. Lett. **38**, 5212–5215 (2013).

139. K. Wu, X. Zhang, J. Wang, and J. Chen, "463-MHz fundamental mode-locked fiber laser based on few-layer MoS$_2$ saturable absorber," Opt. Lett. **40**, 1374–1377 (2015).

140. J. Koo, J. Park, J. Lee, Y. M. Jhon, and J. H. Lee, "Femtosecond harmonic mode-locking of a fiber laser at 3.27 GHz using a bulk-like, MoSe$_2$-based saturable absorber," Opt. Express **24**, 10575–10589 (2016).

141. M. Pawliszewska, Y. Ge, Z. Li, H. Zhang, and J. Sotor, "Fundamental and harmonic mode-locking at 2.1 μm with black phosphorus saturable absorber," Opt. Express **25**, 16916–16921 (2017).

142. J. Kim and Y. Song, "Ultralow-noise mode-locked fiber lasers and frequency combs: principles, status, and applications," Adv. Opt. Photon. **8**, 465–540 (2016).

143. N. Picqué and T. W. Hänsch, "Frequency comb spectroscopy," Nat. Photonics **13**, 146–157 (2019).

144. G. Soboń, P. R. Kaczmarek, D. Sliwinska, J. Sotor, and K. M. Abramski, "High-power fiber-based femtosecond CPA system at 1560 nm," IEEE J. Sel. Top. Quantum Electron. **20**, 492–495 (2014).

145. P. Yan, Z. Jiang, H. Chen, J. Yin, J. Lai, J. Wang, T. He, and J. Yang, "α-In$_2$Se$_3$ wideband optical modulator for pulsed fiber lasers," Opt. Lett. **43**, 4417–4420 (2018).

146. J. Wang, Z. Jiang, H. Chen, J. Li, J. Yin, J. Wang, T. He, P. Yan, and S. Ruan, "High energy soliton pulse generation by a magnetron-sputtering-deposition-grown MoTe$_2$ saturable absorber," Photon. Res. **6**, 535–541 (2018).

147. J. Wang, J. Yin, T. He, and P. Yan, "Sb$_2$Te$_3$ mode-locked ultrafast fiber laser at 1.93 μm," Chin. Phys. B **27**, 084214 (2018).

148. J. Wang, Z. Jiang, H. Chen, J. Li, J. Yin, J. Wang, T. He, P. Yan, and S. Ruan, "Magnetron-sputtering deposited WTe$_2$ for an ultrafast thulium-doped fiber laser," Opt. Lett. **42**, 5010–5013 (2017).

149. J. Sotor, G. Soboń, J. Tarka, I. Pasternak, A. Krajewska, W. Strupinski, and K. M. Abramski, "Passive synchronization of erbium and thulium doped fiber mode-locked lasers enhanced by common graphene saturable absorber," Opt. Express **22**, 5536–5543 (2014).

150. J. Sotor, T. Martynkien, P. G. Schunemann, P. Mergo, L. Rutkowski, and G. Soboń, "All-fiber mid-infrared source tunable from 6 to 9 μm based on difference frequency generation in OP-GaP crystal," Opt. Express **26**, 11756–11763 (2018).

151. P. Ryczkowski, M. Närhi, C. Billet, J. M. Merolla, G. Genty, and J. M. Dudley, "Real-time full-field characterization of transient dissipative soliton dynamics in a mode-locked laser," Nat. Photonics **12**, 221–227 (2018).

152. J. Peng, M. Sorokina, S. Sugavanam, N. Tarasov, D. V. Churkin, S. K. Turitsyn, and H. Zeng, "Real-time observation of dissipative soliton formation in nonlinear polarization rotation mode-locked fibre lasers," Commun. Phys. **1**, 20 (2018).

153. X. Liu, X. Yao, and Y. Cui, "Real-time observation of the buildup of soliton molecules," Phys. Rev. Lett. **121**, 023905 (2018).

154. Y. Cui and X. Liu, "Revelation of the birth and extinction dynamics of solitons in SWNT-mode-locked fiber lasers," Photon. Res. **7**, 423–430 (2019).

155. X. Yi, Q. F. Yang, K. Y. Yang, and K. Vahala, "Imaging soliton dynamics in optical microcavities," Nat. Commun. **9**, 3565 (2018).

156. P. Guo, J. Xu, K. Gong, X. Shen, Y. Lu, Y. Qiu, J. Xu, Z. Zou, C. Wang, H. Yan, Y. Luo, A. Pan, H. Zhang, J. C. Ho, and K. M. Yu, "On-nanowire axial heterojunction design for high-performance photodetectors," ACS Nano **10**, 8474–8481 (2016).

157. X. Ren, Z. Li, Z. Huang, D. Sang, H. Qiao, X. Qi, J. Li, J. Zhong, and H. Zhang, "Environmentally robust black phosphorus nanosheets in solution: application for self-powered photodetector," Adv. Funct. Mater. **27**, 1606834 (2017).

158. Z. Huang, W. Han, H. Tang, L. Ren, D. S. Chander, X. Qi, and H. Zhang, "Photoelectrochemical-type sunlight photodetector based on MoS$_2$/graphene heterostructure," 2D Mater. **2**, 035011 (2015).

159. T. Jiang, Y. Zang, H. Sun, X. Zheng, Y. Liu, Y. Gong, L. Fang, X. A. Cheng, and K. He, "Broadband high-responsivity photodetectors based on large-scale topological crystalline insulator SnTe ultrathin film grown by molecular beam epitaxy," Adv. Opt. Mater. **5**, 1600727 (2017).

160. H. Sun, T. Jiang, Y. Zang, X. Zheng, Y. Gong, Y. Yan, Z. Xu, Y. Liu, L. Fang, and X. A. Cheng, "Broadband ultrafast photovoltaic detectors based on large-scale topological insulator Sb$_2$Te$_3$/STO heterostructures," Nanoscale **9**, 9325–9332 (2017).

161. S. Bai, C. Sun, H. Yan, X. Sun, H. Zhang, L. Luo, X. Lei, P. Wan, and X. Chen, "Healable, transparent, room-temperature electronic sensors based on carbon nanotube network-coated polyelectrolyte multilayers," Small **11**, 5807–5813 (2015).

162. P. Wan, X. Wen, C. Sun, B. K. Chandran, H. Zhang, X. Sun, and X. Chen, "Flexible transparent films based on nanocomposite networks of polyaniline and carbon nanotubes for high-performance gas sensing," Small **11**, 5409–5415 (2015).

163. T. Wang, Y. Guo, P. Wan, X. Sun, H. Zhang, Z. Yu, and X. Chen, "A flexible transparent colorimetric wrist strap sensor," Nanoscale **9**, 869–874 (2017).

164. T. Wang, Y. Guo, P. Wan, H. Zhang, X. Chen, and X. Sun, "Flexible transparent electronic gas sensors," Small **12**, 3748–3756 (2016).
165. D. Li, H. Xue, M. Qi, Y. Wang, S. Aksimsek, N. Chekurov, W. Kim, C. Li, J. Riikonen, F. Ye, Q. Dai, Z. Ren, J. Bai, T. Hasan, H. Lipsanen, and Z. Sun, "Graphene actively *Q*-switched lasers," 2D Mater. **4**, 025095 (2017).
166. J. Bogusławski, Y. Wang, H. Xue, X. Yang, D. Mao, X. Gan, Z. Ren, J. Zhao, Q. Dai, G. Soboń, J. Sotor, and Z. Sun, "Graphene actively mode-locked lasers," Adv. Funct. Mater. **28**, 1801539 (2018).
167. Y. Wang, W. Huang, C. Wang, J. Guo, F. Zhang, Y. Song, Y. Ge, L. Wu, J. Liu, J. Li, and H. Zhang, "An all-optical, actively *Q*-switched fiber laser by an antimonene-based optical modulator," Laser Photon. Rev. **13**, 1800313 (2019).
168. K.-J. Peng, C.-L. Wu, Y.-H. Lin, H.-Y. Wang, C.-H. Cheng, Y.-C. Chi, and G.-R. Lin, "Saturated evanescent-wave absorption of few-layer graphene-covered side-polished single-mode fiber for all-optical switching," Nanophotonics **7**, 207–215 (2018).
169. Y. Ge, Z. Zhu, Y. Xu, Y. Chen, S. Chen, Z. Liang, Y. Song, Y. Zou, H. Zeng, S. Xu, H. Zhang, and D. Fan, "Broadband nonlinear photoresponse of 2D TiS₂ for ultrashort pulse generation and all-optical thresholding devices," Adv. Opt. Mater. **6**, 1701166 (2018).
170. J. Zheng, X. Tang, Z. Yang, Z. Liang, Y. Chen, K. Wang, Y. Song, Y. Zhang, J. Ji, Y. Liu, D. Fan, and H. Zhang, "Few-layer phosphorene-decorated microfiber for all-optical thresholding and optical modulation," Adv. Opt. Mater. **5**, 1700026 (2017).
171. Y. Wang, W. Huang, J. Zhao, H. Huang, C. Wang, F. Zhang, J. Liu, J. Li, M. Zhang, and H. Zhang, "A bismuthene-based multifunctional all-optical phase and intensity modulator enabled by photothermal effect," J. Mater. Chem. C **7**, 871–878 (2019).
172. Y. Wang, F. Zhang, X. Tang, X. Chen, Y. Chen, W. Huang, Z. Liang, L. Wu, Y. Ge, Y. Song, J. Liu, D. Zhang, J. Li, and H. Zhang, "All-optical phosphorene phase modulator with enhanced stability under ambient conditions," Laser Photon. Rev. **12**, 1800016 (2018).
173. Q. Wu, S. Chen, Y. Wang, L. Wu, X. Jiang, F. Zhang, X. Jin, Q. Jiang, Z. Zheng, J. Li, M. Zhang, and H. Zhang, "MZI-based all-optical modulator using MXene Ti₃C₂Tₓ (T = F, O, or OH) deposited microfiber," Adv. Mater. Technol. **4**, 1800532 (2019).
174. J. Zheng, Z. Yang, C. Si, Z. Liang, X. Chen, R. Cao, Z. Guo, K. Wang, Y. Zhang, J. Ji, M. Zhang, D. Fan, and H. Zhang, "Black phosphorus based all-optical-signal-processing: toward high performances and enhanced stability," ACS Photon. **4**, 1466–1476 (2017).
175. S. Chen, L. Miao, X. Chen, Y. Chen, C. Zhao, S. Datta, Y. Li, Q. Bao, H. Zhang, Y. Liu, S. Wen, and D. Fan, "Few-layer topological insulator for all-optical signal processing using the nonlinear Kerr effect," Adv. Opt. Mater. **3**, 1769–1778 (2015).